Guaranteeing a Bounded Tracking Error for Angular Position in Servo Systems Control Based on a Robust Sliding-Based Controller

Xiaohui Yu*‡, Chengge Jia**, Yue Zhao*

*College of Mechanical and Automotive Engineering, College of Humanities & Information Changchun University of Technology, Changchun, Jilin, 130000, China

**Manufacturing Engineering Department, Cosma Automotive (Shanghai) Co., Ltd Changchun Branch, Changchun, Jilin, 130000, China

(13844196836@163.com, 15543272513@163.com m15944169971@163.com)

‡Corresponding Author; Xiaohui Yu, 13844196836@163.com

Received: 05.02.2026 Accepted: 22.04.2026

Abstract- In the angular position control of servo systems, the issue of ensuring the Convergence (CVG) of the Tracking Error (TE) to a small and limited bound, as well as the chattering issue, are two important challenges. This paper addresses this challenge by presenting a new controller from the Sliding Mode Control (SMC) family. In this new controller, a new Reaching Law (RL) is used, in which a function based on the Barrier Function (BF) is used. The issue is that the tracking target, under any initial conditions, eventually converges to a small and limited bound, which is adjusted by the designer. In addition, this RL is robust to Model Uncertainties (MU), providing a robust performance for controlling the position of this machine. The stability of this controller is proven by Lyapunov theory, during which the CVG of the TE to a limited bound is guaranteed. In addition, this controller has the ability to decrease the chattering phenomenon to a good extent. A series of practical tests was conducted in the laboratory to examine the performance of the Proposed Method (PM), and the results confirmed its effectiveness in the above-mentioned field.

Keywords Servo system, control, angular position, barrier, reaching law, convergence.

Nomenclature

Parameter	Description	Parameter	Description
$\boldsymbol{a}$ and $\boldsymbol{b}$	Functions related to tracking error dynamic of rotor angle	R	Stator resistance
$\boldsymbol{c}$, $\boldsymbol{k}$, and $\boldsymbol{\gamma}$	Reaching law parameters	s	Sliding surface
$\boldsymbol{d}$	Uncertainty term	$sign$	Sign function
$\boldsymbol{d^*}$	Upper bound of Uncertainty term	T_e	Electromagnetic torque
$\boldsymbol{e}$	Angle tracking error	T_L	Load torque
$\boldsymbol{f_1}$	Convergence function	t_s	Settling time
$\boldsymbol{f_2}$	Barrier function	u	Control law
$\boldsymbol{i_d}$ and $\boldsymbol{i_q}$	Stator currents in dq-axes	V_1 and V_2	Candidate Lyapunov functions
$\boldsymbol{K}$	Viscous friction constant	v_d and v_q	Stator voltages in dq-axes
$\boldsymbol{K_n}$	Rated values of K	θ	Rotor angle
$\boldsymbol{L_d}$ and $\boldsymbol{L_q}$	Stator inductances in dq-axes	θ^*	Desired rotor angle
$\boldsymbol{M}$	Moment of inertia	ω_m	Angular velocity of the rotor
$\boldsymbol{M_n}$	Rated values of M	φ_f	Rotor flux linkage
$\boldsymbol{m}$, $\boldsymbol{n}$, and $\boldsymbol{\lambda}$	Sliding mode parameters	ΔK	Variations of K
$\boldsymbol{n_p}$	Pole pairs	ΔM	Variations of M

1. Introduction

The increasing adoption of Synchronous Machines (SMs) in servo mechanisms is well documented in industry, robotics, aerospace, and precision manufacturing. This interest is due to their high efficiency, fast dynamic response, and close positional accuracy. In order to achieve accurate position control in these tasks and applications, process analysis and improved control algorithms are necessary to accommodate nonlinearities, parameter changes, and disturbance effects of the SM and the system/environment. A variety of control methodologies, including classical linear controllers, and advanced nonlinear and intelligent strategies, have been developed and refined for SM-based servo systems [1], [2].

The initial control structures used to provide SM position control were classical linear regulators (e.g., Proportional-Integral-Derivative (PID) controllers) that value simplicity, ease of implementation, and fair performance when the system dynamics are simple and stable [3]. Usually, the error signal for the position is regulated via PID, and then the required torque or voltage commands are generated. Although PID controllers can be tuned for acceptable transient and steady-state performance, they have limitations for the management of nonlinearities, variation in parameters, and external disturbances generally experienced by an SM system. The net result is that the implementation of PID controllers is restricted to systems with predictable linear-like behaviors or where the acceptable accuracy standards are modest [4], [5].

Developments in control strategies soon yielded Field-Oriented Control (FOC) [6], a.k.a vector control, and heralded the utilization of SM servo systems for high-performance positioning. FOC dexterously leveraged the mathematical decoupling of the stator currents into meaningful orthogonal direct (d) and quadrature (q) components, the d-axis aligned to the rotor flux. This allows the decoupled regulation of flux and torque - thereby allowing the SM to function similarly to a controllable DC machine under true ideal conditions. FOC encompasses the coordinate transformation (Clarke and Park transforms) and the use of complex current regulators, often implemented as PID or PI controllers that control the direct and quadrature current components [7]. As it relates to position control, FOC combines an outer-loop position and velocity controller, typically using PI controllers, with inner-current loop controllers to provide high-bandwidth current regulation. The combination of current, velocity, and position controllers provides a multi-layered control system that provides fast dynamic response and accurate position control under changing load conditions. The high fidelity of FOC in representing actual machine dynamics makes it ideal for servo machine applications that require high accuracy, response, and robustness. The extraordinary flexibility allowed by the inherent structure of FOC means that most can be implemented using sensorless techniques, such as observers, that take away costs and environmental factors, such as the requirement for a rotor position sensor. Sensorless FOC methods, such as observer techniques, on the basis of back-EMF or flux observers, can be implemented to estimate rotor position and/or velocity in Real-Time (RT), and these approaches will allow FOC to be successful in control situations without recovering direct rotor position feedback [8], [9].

The purpose of sensorless control strategies [10] is to remove the mechanical sensors (e.g., encoders or resolver systems) that add complexity and cost and are also sensitive to the environment. The development of techniques, namely, Extended Kalman Filters (EKF) [11], Sliding Mode Observers (SMO) [12], and Voltage-Model-Based Observers, are each observer-based algorithms that directly estimate rotor position and speed from electrical measurements; this allows the controller to maintain full function without feedback of the rotor. Sensorless FOC then offers an attractive route for performance in servo systems where cost and robustness for quality and durability are important. The difficulty for sensorless approaches is maintaining estimation accuracy when in low-speed operation or standstill, where back-emf (Electro-Motive-Force) signals are weak. More recently, developments that help with this can call upon advanced observer designs and adaptive algorithms, whilst some observers may incorporate hybrid designs that operate in sensorless control and maintain limited sensor feedback for low-speed performance.

Model Predictive Control (MPC) [13] has become an increasingly attractive modern control strategy for SM servo systems because it can explicitly handle multivariable interactions, constraints, and nonlinearities. The essential workings of MPC are to repeatedly solve an optimal control problem over a finite prediction horizon using the mathematical model of the SM, producing control actions that will minimize an objective cost function. When applied to SMs, MPC can manage position, velocity, and current control states at the same time with constraints on inverter voltages, currents, or thermal limits [14]. MPC is applied to a wide variety of SM position control systems, and usually involves discretizing the system dynamics and using an algorithm, often Quadratic Programming (QP), to calculate the optimal voltage inputs. MPC's ability to forecast allows it to control anticipated trajectories, improving transient performance and disturbances. MPC is also customarily very computation-intensive, requiring dedicated hardware and algorithms, limiting its use in RT embedded systems. New developments in computational hardware and solver algorithms will ultimately allow MPC to have higher utility in a high-performance servo-system [15].

Due to the inherent nonlinearity and uncertainty of SMs, and particularly due to variations in parameters and disturbances from the environment, robust controllers such as SMC [16] have drawn interest. With SMC, control laws are synthesized to direct all system trajectories onto a defined sliding surface; thereby guaranteeing that dynamic characteristics are achieved under uncertainty. In SM position control, SMC leads to very robust performance, maintaining position even with parameter variations caused by temperature, saturation of the machine, or load changes [17]. In SMC, a suitable sliding surface is established on the basis of the position error, and a discontinuous control law is derived that confines the system state motion to slide along this surface. To avoid undesirable chattering, boundary layer methods or higher-order sliding mode methods are used. Many of the robust control approaches presented here utilize adaptive control schemes, allowing for changes in parameters to maximize operation under actual operating conditions [18].

With the awareness that controller systems must tolerate uncertainties and variations, and that the adaptive control methods [19] have been injected into the SM position control methods. Adaptive controllers typically modify their tuning parameters in RT with respect to the discovered system's state or identified model to retain the best performance. Self-Tuning Regulators (STR) and Model Reference Adaptive Control (MRAC) have been incorporated to counter parameter drift or uncertainties regarding the SM parameters supporting the ux linkage or inertia [20]. In more recent developments, intelligent control algorithms, including fuzzy logic controllers [21], neural networks [22], and hybrid structures that utilize both traditional approaches and learning-based approaches (from human experience), have recently gained active attention within the SM position control domain. Neural networks are able to adaptively approximate nonlinearities and uncertainty as they learn, resulting in some uncertainty and more robustness and accuracy. Fuzzy logic controllers provide another set of approaches that encode expert knowledge and manage nonlinearities in a setting that does not require an explicit mathematical model, often yielding smoother control similar to a human operator.

Due to the many strengths and weaknesses of each individual control approach, hybrid control schemes that make use of more than one control approach have been explored to conform to the demanding specifications of modern servo systems. FOC and SMC can offer robustness that each individual approach cannot alone, while neural network-based observers can be used along with MPC in order to increase estimation accuracy and predictive capability. Many hybrid schemes utilize adaptive strategies that maintain or change control mode based on operational scenarios, e.g., low speed versus high load, to assure desired performance [23]. Advancements in hardware, including Digital Signal Processors (DSPs) and Field-Programmable Gate Arrays (FPGAs), have allowed the RT implementation of complex hybrid algorithms, thereby expanding the practical use of these algorithms in highly accurate servo systems. These multi-control architecture methods are designed to combine the fast dynamic response and robustness of nonlinear controllers, accuracy of model-based control schemes, and adaptability of learning algorithms [24], [25].

This work addressed two fundamental issues in the position control of SMs: the error must converge to a small bounded region, and chatter must be reduced. The PM in this document is a new SMC strategy that relies on the new SMC-RL related to a barrier–function–style expression. The suggested design guarantees that the error converges to a small bound that can be tuned by the designer, regardless of the starting condition. The RL is also robust to MU, demonstrating dependable performance in position control. Lyapunov theory was used to prove the controller's stability, showing that the TE reaches the prescribed bound within a finite time. More so, the PM achieved satisfactory chatter reduction. Finally, experimental testing in a lab setting demonstrated the PM's overall efficacy in emulating what is intended by bounded CVG and in improving chatter under real-world scenarios.

In the second part, the modeling of the desired system will be presented, and then in the third part, the desired control method will be formulated. After presenting the results of practical experiments and their analysis in Section 4, the document's conclusions will be presented in Section 5.

2. Modelling the Servo System

A servo system consists of an electrical machine and a control circuit. The electrical machine studied in this paper is a permanent magnet SM, which is shown in Fig. 1. This machine features a rotor with permanent magnets that create the magnetic flux, while the stator contains three-phase windings that generate a rotating magnetic field. The rotor tracks this field in synchrony, preserving a steady electrical-to-mechanical angle. As a result, it offers high efficiency, strong power density, and rapid dynamic performance, finding widespread use in precision drives, robotics, CNC systems, and electric vehicles.

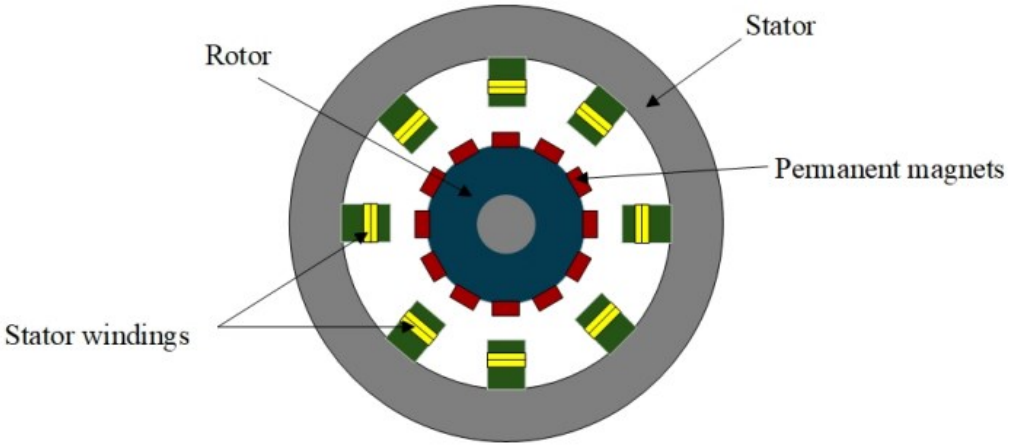

Fig. 1. The structure of the electrical machine in the servo system.

The dynamic behavior associated with stator voltages and currents in the dq-axes is described as [26]:

$$v_d = L_d i_d + R i_d + n\omega_m L_q i_q$$
$$v_q = L_q i_q + R i_q + n\omega_m (L_d i_d + \varphi_f) \quad (1)$$

Here, L_d and L_q denotes the stator inductances in dq-axes; ω_m signifies the angular velocity of the rotor; φ_f refers to the rotor flux linkage; R refers to the stator resistance; i_d, i_q, v_d, and v_q respectively indicate the stator currents and

voltages in the dq-axes; n represents the pole pairs. The dynamic behavior associated with the rotor motor is described as [26]:

$$M\ddot{\theta} = T_e - T_L - K\omega_m \quad (2)$$

Where T_e refers to the electromagnetic torque; K refers to the viscous friction constant; M denotes the moment of inertia; T_L refers to the load torque; T_e is calculated as [26]:

$$T_e = 1.5ni_q(i_d\,(L_d - L_q) + \varphi_f) \quad (3)$$

For a surface-mounted servo system, $L_d = L_q$ is obtained. Therefore, it is concluded that:

$$T_e = 1.5ni_q\varphi_f \quad (4)$$

Integrating Eqs. (2) and (4):

$$M\ddot{\theta} = 1.5ni_q\varphi_f - T_L - K\omega_m \quad (5)$$

By considering the uncertainty and disturbance effects in practical applications, the following can be written:

$$\begin{aligned}&(M_n + \Delta M)\ddot{\theta} = 1.5ni_q\varphi_f - T_L - (K_n + \Delta K)\omega_m\\ &\Rightarrow M_n\ddot{\theta} = 1.5ni_q\varphi_f - T_L - K_n\omega_m - \Delta M\ddot{\theta} - \Delta K\omega_m\\ &\Rightarrow \ddot{\theta} = 1.5{M_n}^{-1}ni_q\varphi_f - {M_n}^{-1}T_L - {M_n}^{-1}K_n\omega_m\\ &\qquad - {M_n}^{-1}\Delta M\ddot{\theta} - {M_n}^{-1}\Delta K\omega_m\end{aligned} \quad (6)$$

Where ΔM and ΔK are the variations of M and K, respectively; M_n and K_n are the rated values of M_n and K_n, respectively. By defining:

$$d = -{M_n}^{-1}T_L - {M_n}^{-1}\Delta M\ddot{\theta} - {M_n}^{-1}\Delta K\omega_m \quad (7)$$

$$a = 1.5{M_n}^{-1}n\varphi_f \quad (8)$$

$$b = -{M_n}^{-1}K_n\omega_m \quad (9)$$

$$u = i_q \quad (10)$$

Eq. (6) is rewritten:

$$\ddot{\theta} = au + b + d \quad (11)$$

Let θ^* denote the desired angle. By defining $e = \theta - \theta^*$, the following is obtained:

$$\ddot{e} = au + b + d - \ddot{\theta}^* \quad (12)$$

3. Servo System Controller Design

The control circuit of a servo system is depicted in Fig. 2. In this circuit, the stator reference current in the q-axis is produced by a control law. Subsequently, the stator voltages in the dq-axes are generated by PI controllers. These voltages are then converted to the three-phase voltage required by the machine through several interface circuits, including $dq/\alpha\beta$ converter, SVPWM, and an inverter.

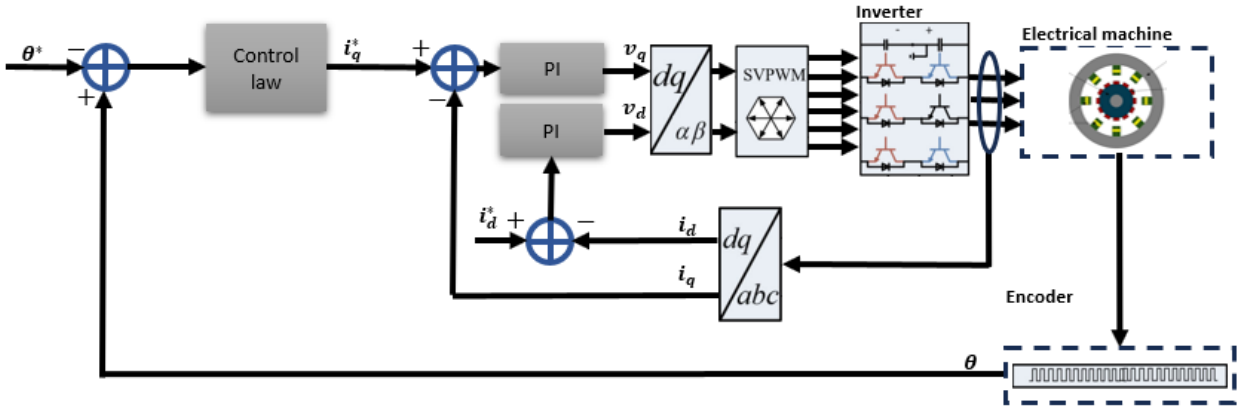

Fig. 2. The control circuit of the servo system.

The appropriate control law for generating the stator reference current in the q-axis to achieve the desired angle tracking performance is highly critical. Therefore, in this study, a control law based on a fast-sliding surface and a BF is designed so that the tracking speed is increased and robustness to uncertainties is obtained. Accordingly, the proposed sliding surface is described as:

$$s = \dot{e} + me + n|e|^{\lambda}sign(e) \quad (13)$$

Where $m > 0$, $n > 0$, and $0 < \lambda < 1$ are sliding surface parameters. If e is located on the sliding surface, the duration required for e to approach zero is computed as follows:

$$\begin{aligned}&s = 0 \Rightarrow \dot{e} + me + n|e|^{\lambda}sign(e) = 0 \Rightarrow \dot{e}\\ &\qquad = -me - n|e|^{\lambda}\,sign(e)\\ &\Rightarrow dt = \frac{1}{-me - n|e|^{\lambda}\,sign(e)}de\end{aligned} \quad (14)$$

By integrating both sides of Eq. (14) from 0 to t_s:

$$\int_0^{t_s} dt = \int_{|e(0)|}^{0} \frac{1}{-me - n|e|^{\lambda}\,sign(e)}de \quad (15)$$

$$\Rightarrow t_s = \int_0^{|e(0)|} \frac{1}{me + ne^{\lambda}}de$$

me in Eq. (15) causes t_s for the proposed sliding surface to be smaller than t_s for a conventional terminal sliding surface.

$$u = u_1 + u_2 \quad (16)$$

Where:

$$u_1 = \frac{-b + \ddot{\theta}^* - m\dot{e} - n\lambda|e|^{\lambda-1}\dot{e}}{a} \quad (17)$$

$$u_2 = \frac{-f\,sign(s) - ks}{a} \quad (18)$$

In Eq. (18), $k > 0$ is determined by the designer and f is calculated as:

$$f = \begin{cases} f_1, |s| \geq \gamma \\ f_2, |s| < \gamma \end{cases} \quad (19)$$

Where:

$$\dot{f}_1 = c|s| \quad (20)$$

$$f_2 = \frac{|s|}{\gamma - |s|} \quad (21)$$

$\gamma > 0$ is the boundary of functions, c is a tuning parameter, and f_2 is a BF.

Using Eqs. (12), (13), and (16), $\dot{s}$ is:

$$\begin{aligned}\dot{s} &= \ddot{e} + m\dot{e} + n\lambda|e|^{\lambda-1}\dot{e} \\ &= au + b + d - \ddot{\theta}^* + m\dot{e} + n\lambda|e|^{\lambda-1}\dot{e} \\ &= a\left(\frac{-b + \ddot{\theta}^* - m\dot{e} - n\lambda|e|^{\lambda-1}\dot{e}}{a} + \frac{-f\,sign(s) - ks}{a}\right) + b + d \\ &\quad - \ddot{\theta}^* + m\dot{e} + n\lambda|e|^{\lambda-1}\dot{e} \\ &= -f\,sign(s) - ks + d\end{aligned} \tag{22}$$

The stability of the closed-loop system can be assessed in 2 separate scenarios, which are detailed in the following sections:

C1: $|s| \geq \gamma$. The Lyapunov function is intended:

$$V_1 = 0.5s^2 + 0.5c^{-1}(f_1 - d^*)^2 \tag{23}$$

Where $|d| \leq d^*$. $\dot{V}_1$ is:

$$\begin{aligned}\dot{V}_1 &= s\dot{s} + c^{-1}(f_1 - d^*)\dot{f}_1 \\ &= s(d - f_1\,sign(s) - ks) + c^{-1}(f_1 - d^*)(c|s|) \\ &= -sd - f_1|s| - ks^2 + f_1|s| - d^*|s| \\ &\leq d^*|s| - f_1|s| - ks^2 + f_1|s| - d^*|s| < 0\end{aligned} \tag{24}$$

$\dot{V}_1 < 0$ shows that s reach the region where $|s| < \gamma$.

C2: $|s| < \gamma$. The Lyapunov function is intended:

$$V_2 = 0.5s^2 + 0.5{f_2}^2 \tag{25}$$

$\dot{V}_2$ is:

$$\begin{aligned}\dot{V}_2 &= s\dot{s} + f_2\dot{f}_2 \\ &= s(d - f_2 sign(s) - ks) + f_2\frac{\gamma\, sgn(s)}{(\gamma - |s|)^2}(d - f_2 sign(s) - ks) \\ &\leq (d^* - f_2)|s| - ks^2 + f_2\frac{\gamma}{(\gamma - |s|)^2}(d^* - f_2 - k|s|)\end{aligned} \tag{26}$$

Let $s_1 = \gamma(\frac{d^*}{d^*+1})$. If $s_1 \leq |s| < \gamma$, then $f_2(s) > f_2(s_1) = d^*$, and consequently, $\dot{V}_2 < 0$. The condition $\dot{V}_2 < 0$ indicates that s reaches the region where $s_1 \leq |s| < \gamma$.

Remark 1. By choosing an appropriate γ, the angle TE can be reduced in the presence of MU.

Remark 2. The following guideline demonstrates how sliding surface parameter choices affect control outcomes and assist in adjusting the parameters.

1. According to Eqs. (15)-(18), the larger value of m leads to lower value of t_s, but the value of u increases. So, we increase this value from 0 until the value of u saturates.
2. According to Eqs. (15)-(18), the larger value of n leads to lower value of t_s, but the value of u increases. So, we increase this value from 0 until the value of u saturates.
3. According to Eqs. (15)-(18), the larger value of λleads to smaller value of overshoot percentage, but the value of u increases. So, we increase this value from 0 until the value of u saturates.

Remark 3. In existing sliding mode controllers, increasing robustness leads to a higher level of chattering and a reduction in control performance. Moreover, their convergence region for guaranteeing a predefined bound of tracking error is unknown. Therefore, in this study, a new reaching law based on the barrier function is proposed to both provide high robustness with a low level of chattering and drive the tracking error to a predefined bound while maintaining desirable performance. It should be noted that the convergence region can be adjusted by the designer. On the other hand, a new stability proof was carried out to verify the claims made.

Remark 4. By analyzing the effects of k and c on tracking performance in the experimental test, it can be observed that increasing the value of k increases the convergence speed, but the value of u increases. Therefore, the value of k is increased from 0 up to a level where the value of u reaches saturation. Also, increasing the value of c increases the convergence speed, but the value of overshoot percentage increases. Therefore, c is increased up to a level where the value of overshoot percentage exceeds the predetermined bound. Moreover, the value of γ is determined based on the convergence region desired by the designer in order to achieve the required accuracy.

By providing the desired values of c and γ, the functions f_1 and f_2 are determined. The implementation of function f_2 in Eq. (21) on the processor is straightforward. Function $f_1$in Eq. (20) is implemented on the processor using an integrator with zero initial condition ($f_1 = \int c|s|\,dt$).

Remark 5. Due to function f, the stability analysis is carried out in two regions, $C1$ and $C2$. The stability analysis in region $C1$ guarantees that s eventually reaches region $C2$. Then, the stability analysis in region $C2$ ensures that s remains within region $C2$. This analysis shows that as the values of γ and d^* decrease, region $C2$ becomes smaller and the tracking accuracy improves; however, the robustness of the controller against uncertainties decreases and the magnitude of the control law becomes larger. Therefore, the parameters γ and d^* introduce a level of conservativeness in the analysis. To reduce this conservativeness, an estimator can be designed to compute d, although this would increase the computational complexity.

4. Experiments

A set of experimental evaluations was carried out to assess the effectiveness of the suggested algorithm. The performance of the PM was then contrasted with the Terminal Sliding Mode Control (TSMC) technique, utilizing the experimental configuration depicted in Fig. 3. The experimental test configuration for the position control of the SM servo system includes a handful of components that have been chosen for reliability and performance. In this setup, the SM (often modeled as a Siemens 1FT7 series, such as Siemens 1FT7 301-1AB00-0AA0) acts as the primary moving component because it is a robust system that provides good torque and precise position control. The power source to the SM is a high-quality inverter, in this application, the Texas Instruments UCC5320, which provides high-frequency pulse width modulation (PWM) characteristics and thus an even and efficient voltage supply. To get the best measurement of the position of the shaft of the machine, the encoder is a Renishaw RESOLUTE optical encoder (RESOLUTE 14-bit), which gives a good resolution for each position measurement, something that is necessary for closed-loop control. The control algorithm is applied through a custom DSP, such as the Texas Instruments TMS320F28379D, which has RT processing capabilities required for dynamic control schemes.

The DSP connects to the inverter through a switch driver circuit, for example, the International Rectifier (IR) IR2110 switch driver circuit, which provides the necessary gate signals while providing isolation and protection. A power supply unit (Brinkmann Electric PS100A in this case) provides stable DC voltage to all of the circuitry. A National Instruments (NI) USB-6356 multifunction DAQ records the signals from all of the encoders, current sensors, and voltage sensors used in the experiments. These recorded signals provide the means to perform a detailed assessment of the system performance through measurements. All of the experimentation equipment is connected through a control cabinet that houses all the electrical devices and limits exposure to electromagnetic noise, which is safer and removes interfering voltages for the purpose of measurements. This integration of all features allows the researchers to gather experimental data with precision to reproduce the experimental validity of the positional control of the SM servo system. The controller parameters are provided in Table 1.

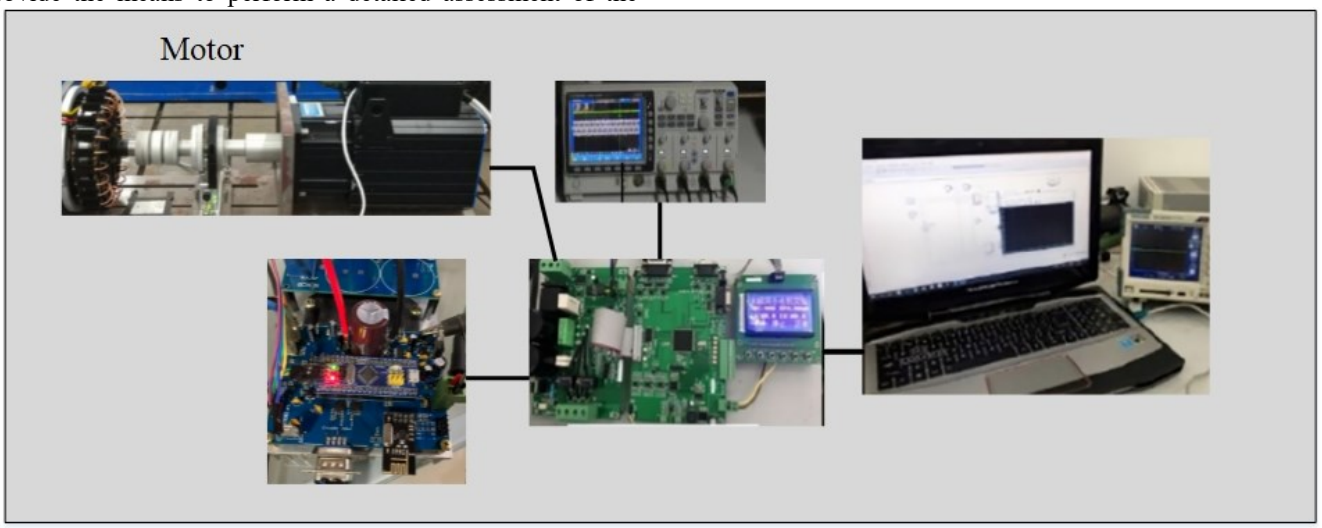

Fig. 3. Test setup.

Table 1. Values of controller parameters

Parameter	Value
m	2
n	3
λ	0.6
k	2
c	0.1
γ	0.01

In the first part of the practical experiments, a setpoint is applied to the machine position as an input to the control loop, and the performance of both methods is examined in steady state. Before the experiments, for easy replication of the work before experimental test the results of a preliminary simulation is resented. As is clear from part A of Fig. 4, the simulation result confirmed the good performance of the proposed method in tracking a multiple step input. The results of these experiments are presented in Fig. 4, and in parts B and C of this figure, the performance of both control methods for tracking the reference position is compared. In the D part of this figure, the control signal, which is a current, is also shown. The data in this figure indicates that the PM achieves considerably improved results. This method has a small jump size of less than 0.5 radians, and its CVG time is less than 0.1 second. Also, the steady-state error is below 0.1 radian. This is while the SMC method has a jump of 1.5 radians and its CVG time is 0.38 seconds. Furthermore, the steady-state error of this technique is also 0.2 radians. Therefore, it can be concluded that in the steady state, where the setpoint is employed as a position to the control loop, the PM performs more accurately and faster. In part E of Fig. 4, the diagram of the motor current is indicated that shows the feasibility of the proposed control method.

By comparing the simulation result to the experimental result, it can be seen that there is a negligible error in the experimental implementing of the proposed method. To be more specific, the proposed method has the jump, CVG, and steady state error of 0.5 rad, 0.1 sec, and0.1 rad, respectively. While in the simulations, these values are 0.4 rad, 0.0.08 sec, and 0.82 rad, respectively.

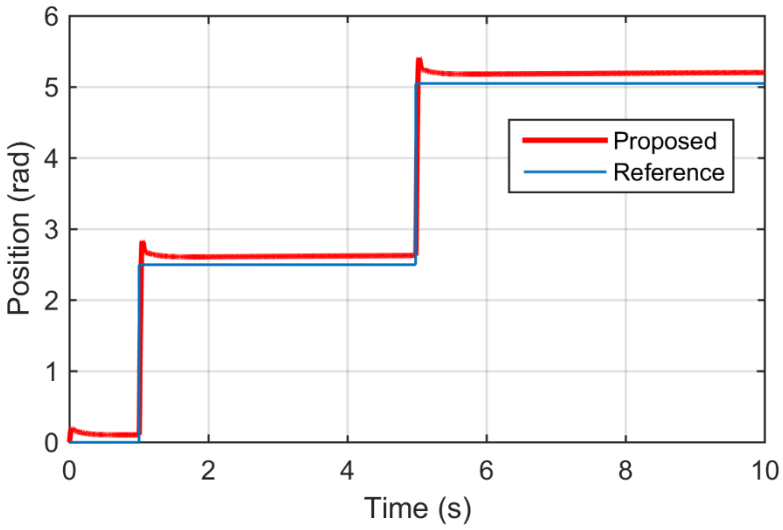
Position (rad)
Time (s)
Proposed
Reference

A

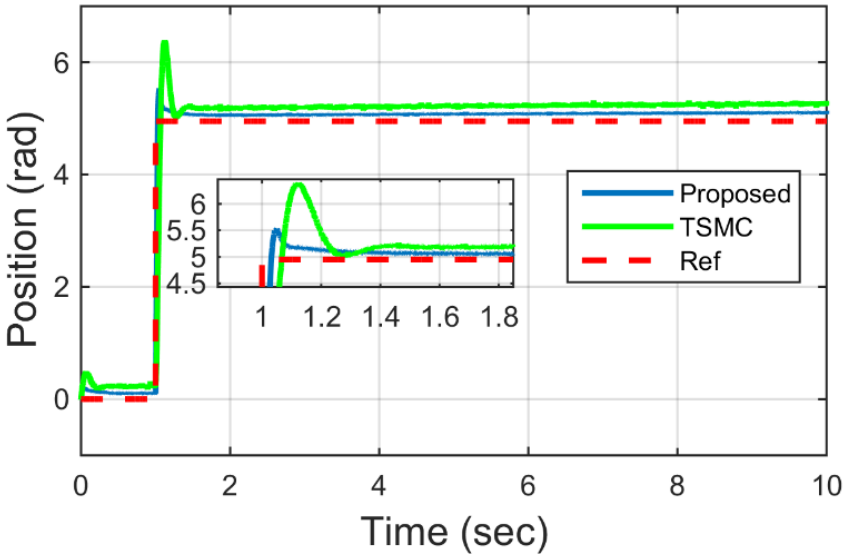
Position (rad)
Time (sec)
Proposed
TSMC
Ref

B

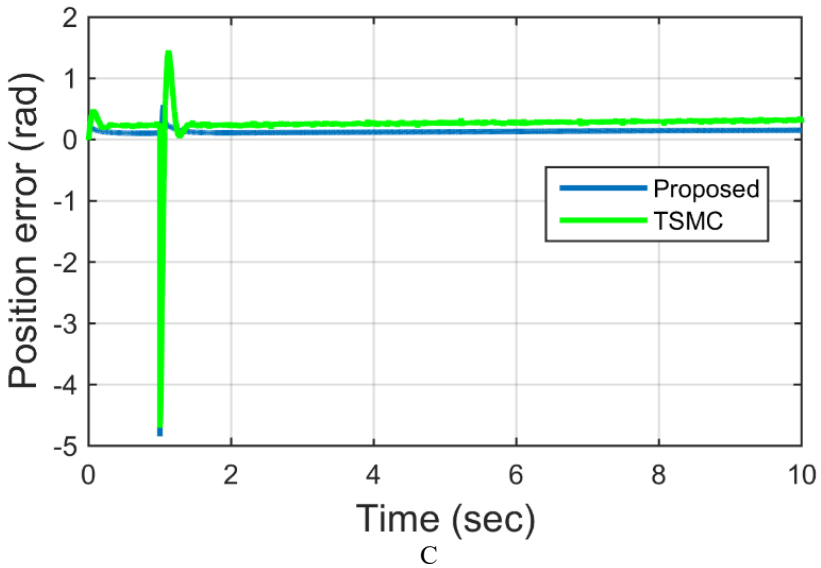
Position error (rad)
Time (sec)
Proposed
TSMC

C

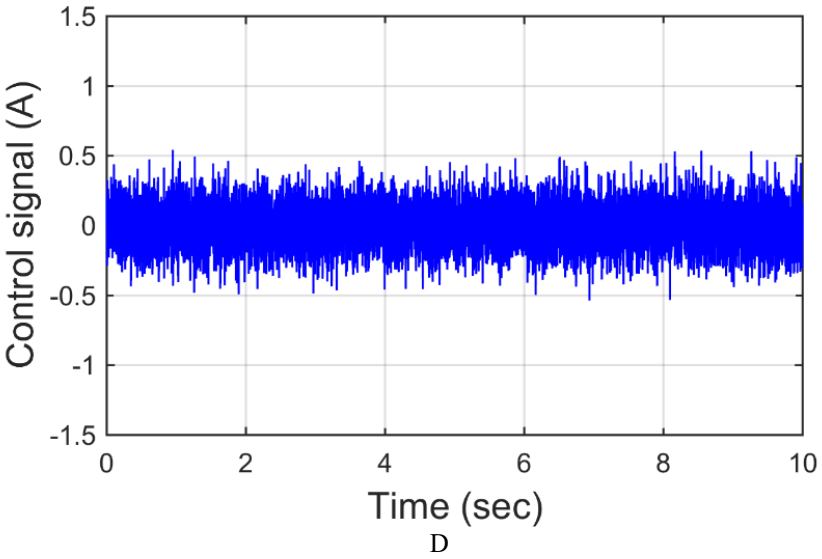

D

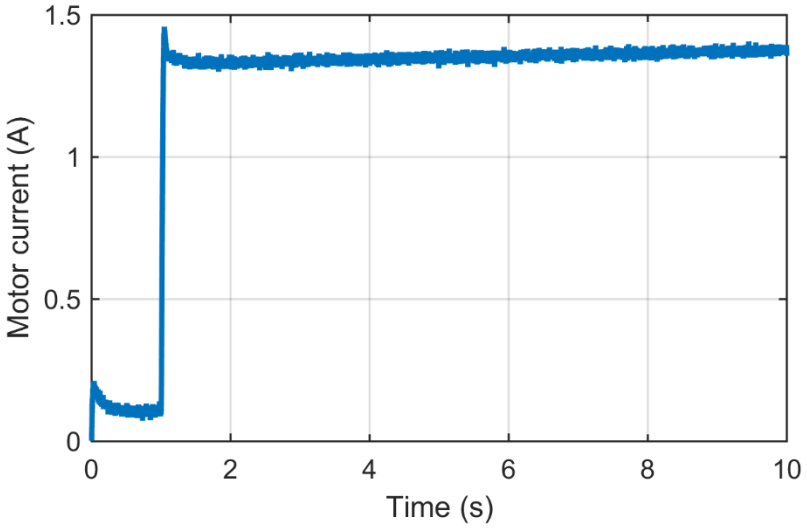

E

Fig. 4. Experiments for the step tracking. A) Simulation result. B) Position. C) Position error. D) Control signal. E) Motor current.

In the second part of the practical tests, the machine reference position is considered as a triangular wave to check the performance of both methods in transient mode and for rotation in two directions at all times during the drive system execution. The findings of these experiments are depicted in Fig. 5, and, as in the previous scenario, the performance results of both methods for tracking the reference position as well as the control signal in this scenario are presented in this figure. As is clear from these figures, the PM has a transient error of 0.1 radian, while the TSMC technique has an error of 0.4 radians. The reason for this is that the SMC method has a longer CVG time of 3 seconds, which causes the TSMC method to lag behind the reference signal during the execution time of the drive system, where the reference position is always changing. As shown in the third part of this figure, the control law generated in this case also attains a reasonable value, indicating that the desired method is feasible. As is shown in part D of Fig. 5, the value of the motor current changes in its value during the change in the direction of the motor.

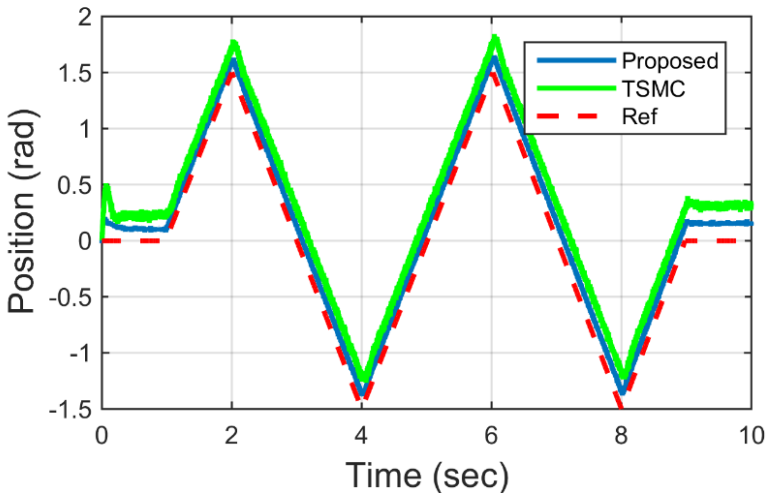
Proposed
TSMC
Ref
Position (rad)
Time (sec)

A

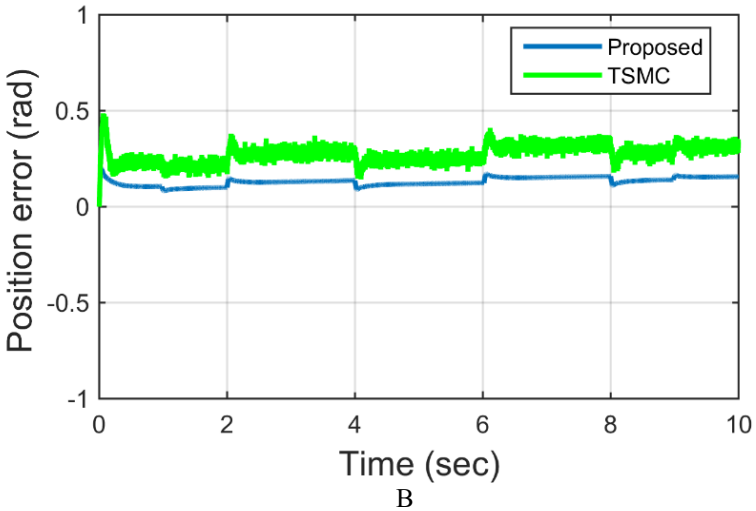
Proposed
TSMC
Position error (rad)
Time (sec)

B

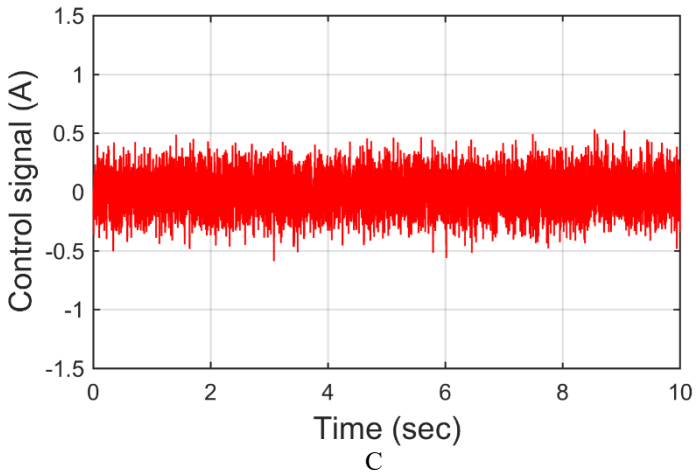
Control signal (A)
Time (sec)

C

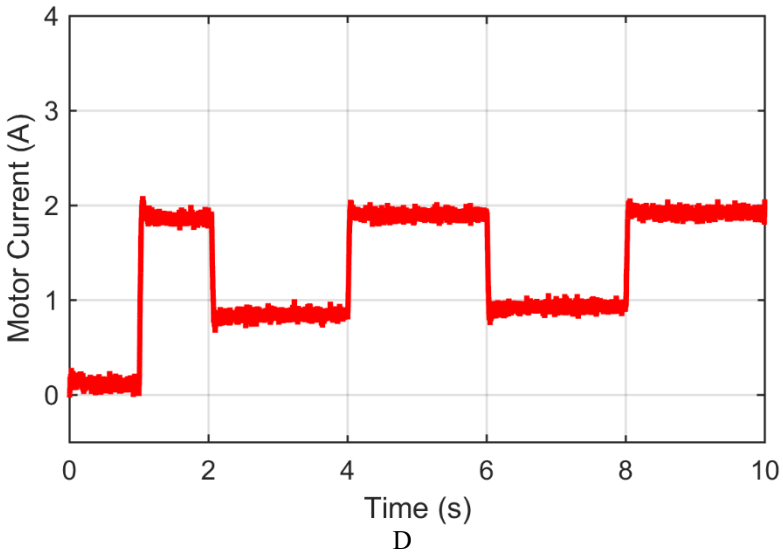

D

Fig. 5. Experiments for the triangle tracking. A) Position. B) Position error. C) Control signal. D) Motor current.

In the final scenario of practical tests, the position applied to the machine is considered as a sine wave. In this case, the performance of both control methods for rotation in both directions is checked. The results of these experiments, along with the generated control signal, are shown in Fig. 6. As is clear from this check, due to the lag of the TSMC method, which results in a longer CVG time of 0.35 seconds in this scenario, there is always a bias of 0.38 radians in the performance of this method. This is while the method considered in this article has a higher CVG speed and its tracking distance is as small as 0.2 radian. In addition, due to the presence of the chattering phenomenon in the TSMC method, there is some fluctuation in its performance in all three scenarios. Therefore, it can be concluded that in this scenario, the performance of the approach in question has higher accuracy, and the higher the frequency of this sine wave, the higher the accuracy of the TSMC method. Part D of Fig. 6 shows the feasibility of the control method confirmed by the reasonable value of the motor current.

The limits of the current and voltage have been considered based on the physical features of the motor and drive system in the experimental tests. To show how close did the proposed method operate to those, the current of the motor and generated control signals have been presented in the paper to show the feasibility of the proposed method. The results confirmed this and the values did not exceed the limitations.

In Table. 2, a comparison between method is reported based on the sine wave frequency. As is clear, both methods have more tracking error by increasing the frequency and the proposed method has an acceptable performance up ti the time period of 1 sec.

Table 2. Tracking error in the sinusoidal reference

Method	Time period		
	3	2	1
Proposed	0.2 rad	0.28 rad	0.37 rad
TSMC	0.38 rad	0.45 rad	0.45 rad

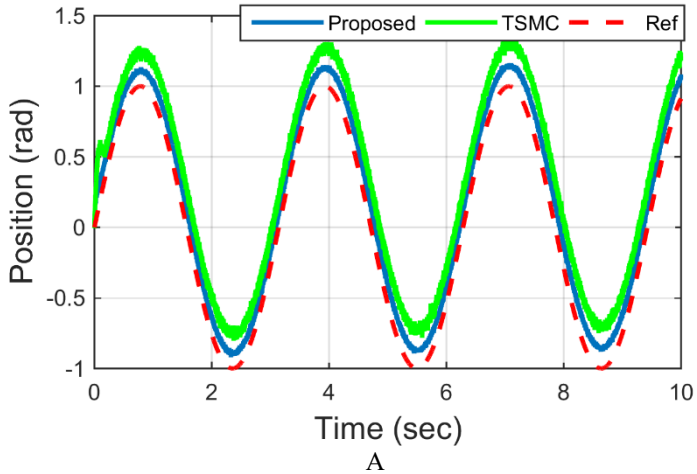

A

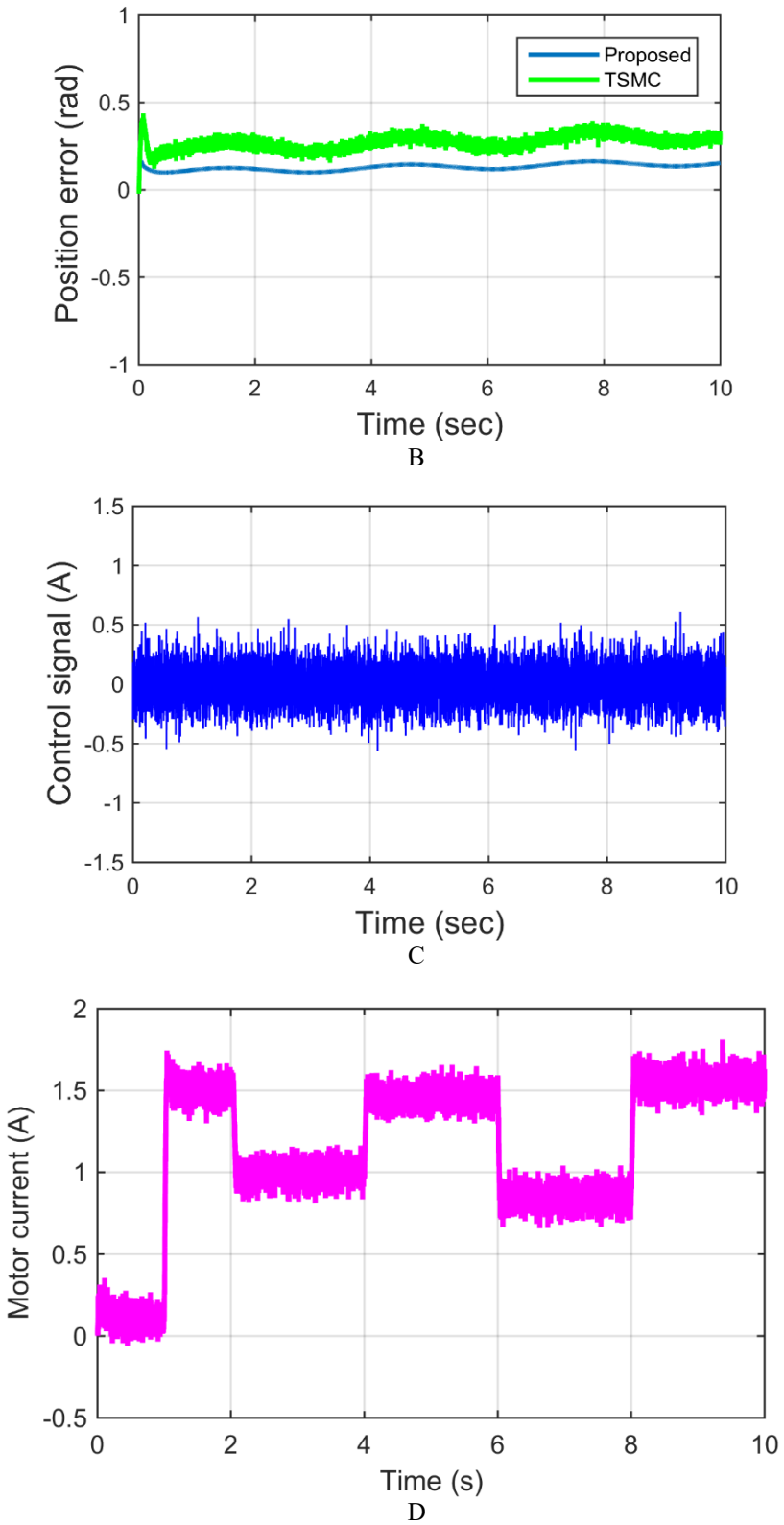

Fig. 6. Experiments for the sine tracking. A) Position. B) Position error. C) Control signal. D) Motor current.

5. Conclusion

In this study, two central challenges of SM positioning control were addressed: the CVG of the TE to a small bounded region, and the reduction of chattering. A SMC approach was presented, which included a novel RL expressed in the form of a barrier-function-type expression. The design guarantees that the TE will converge to a designer-tunable bound at any point in time, regardless of the initial conditions of the system. The reach law is robust to MU, so reliable position-control performance in the system was found regardless of the operational conditions. Lyapunov theory was developed to analyze the stability of the proposed controller, which verified

that the TE converges in a finite time to the user-defined bound. Moreover, the approach accomplished a significant reduction in chattering, thereby providing smoother and realistic behavior in the execution of the real problem. A battery of experimental tests in the laboratory was carried out to validate the approach, confirming the claims of the theory and proving bounded CVG, while additionally showing improvement in chattering with real disturbances and uncertainties present. The results suggested that the proposed PP-SMC approach was a strong, dependable, and scalable approach for precision position control of the SM. As such, it is reasonable to consider potential applications in high-precision motion systems and other industrial applications with stringent tracking accuracy specifications and reduced chattering. In addition, the reasonable values of the motor current confirmed the feasibility of the proposed control method. Future work could address: exploration of parameter tuning schemes and RT implementation on embedded hardware.

Acknowledgement

N/A

Authorship Contribution Statement

Xiaohui Yu: Project administration, Conceptualization, Supervision, Writing-Original draft preparation.
Chengge Jia: Validation, Methodology, Software.
Yue Zhao: Language review, Formal analysis.

Data Availability

Available upon request.

Conflicts of Interest

The authors assert that they have no conflict of interest concerning the release of this article.

References

[1] G. Wang, M. Valla, and J. Solsona, "Position sensorless permanent magnet synchronous machine drives—A review," IEEE Transactions on Industrial Electronics, vol. 67, no. 7, pp. 5830–5842, 2019.

[2] Y. Zhao, C. Wei, Z. Zhang, and W. Qiao, "A review on position/speed sensorless control for permanent-magnet synchronous machine-based wind energy conversion systems," IEEE J. Emerg. Sel. Top. Power Electron., vol. 1, no. 4, pp. 203–216, 2013.

[3] S. Yeh and Y. Chang, "Development of an extended proportional–integral–proportional control for improving positional motion performance of permanent magnet synchronous motor-driven servomechanism," Asian J. Control, vol. 24, no. 6, pp. 2969–2980, 2022.

[4] N. K. Agarwal, M. Prateek, A. Saxena, and G. K. Singh, "A novel design of hybrid fuzzy poisson fractional order proportional integral derivative controller for the wind driven permanent magnet synchronous generator," IEEE Access, vol. 11, pp. 132641–132651, 2023.

[5] S. Khubalkar, A. Junghare, M. Aware, and S. Das, "Modeling and control of a permanent-magnet brushless DC motor drive using a fractional order proportional-integral-derivative controller," Turkish Journal of Electrical Engineering and Computer Sciences, vol. 25, no. 5, pp. 4223–4241, 2017.

[6] T.-D. Ton, M.-F. Hsieh, and P.-H. Chen, "A novel robust sensorless technique for field-oriented control drive of permanent magnet synchronous motor," IEEE Access, vol. 9, pp. 100882–100894, 2021.

[7] V. Zakharov and T. Minav, "Analysis of field oriented control of permanent magnet synchronous motor for a valveless pump-controlled actuator," in Proceedings, MDPI, 2020, p. 19.

[8] R. G. Krishnan, T. B. Isha, and P. Balakrishnan, "A back-EMF based sensorless speed control of permanent magnet synchronous machine," in 2017 International Conference on Circuit, Power and Computing Technologies (ICCPCT), IEEE, 2017, pp. 1–5.

[9] O. Stiscia, M. Slunjski, E. Levi, and A. Cavagnino, "Sensorless control of a nine-phase surface mounted permanent magnet synchronous machine with highly non-sinusoidal back-EMF," in IECON 2019-45th Annual Conference of the IEEE Industrial Electronics Society, IEEE, 2019, pp. 1327–1332.

[10] X. Sun, J. Cao, G. Lei, Y. Guo, and J. Zhu, "Speed sensorless control for permanent magnet synchronous motors based on finite position set," IEEE Transactions on Industrial Electronics, vol. 67, no. 7, pp. 6089–6100, 2019.

[11] R. Dhaouadi, N. Mohan, and L. Norum, "Design and implementation of an extended Kalman filter for the state estimation of a permanent magnet synchronous motor," IEEE Trans. Power Electron., vol. 6, no. 3, pp. 491–497, 1991.

[12] Y. Wang and X. Liu, "Model predictive position control of permanent magnet synchronous motor servo system with sliding mode observer," Asian J. Control, vol. 25, no. 1, pp. 443–461, 2023.

[13] Y. Wei, Y. Wei, Y. Sun, H. Qi, and X. Guo, "Prediction horizons optimized nonlinear predictive control for permanent magnet synchronous motor position system," IEEE Transactions on Industrial Electronics, vol. 67, no. 11, pp. 9153–9163, 2019.

[14] Z. Li, J. An, Q. Zhang, H. Liu, and H. Sun, "Design of PMSLM position controller based on model predictive control algorithm," IEEE Access, vol. 9, pp. 78835–78846, 2021.

[15] M. S. Mubarok and T.-H. Liu, "Implementation of predictive controllers for matrix-converter-based interior permanent magnet synchronous motor position control systems," IEEE J. Emerg. Sel. Top. Power Electron., vol. 7, no. 1, pp. 261–273, 2018.

[16] W. Zhu, D. Chen, H. Du, and X. Wang, "Position control for permanent magnet synchronous motor based on neural network and terminal sliding mode control," Transactions of the Institute of Measurement and Control, vol. 42, no. 9, pp. 1632–1640, 2020.

[17] L. Qi and H. Shi, "Adaptive position tracking control of permanent magnet synchronous motor based on RBF fast terminal sliding mode control," Neurocomputing, vol. 115, pp. 23–30, 2013.

[18] J. Gil, S. You, Y. Lee, and W. Kim, "Super twisting-based nonlinear gain sliding mode controller for position control of permanent-magnet synchronous motors," IEEE Access, vol. 9, pp. 142060–142070, 2021.

[19] T.-H. Liu, H.-T. Pu, and C.-K. Lin, "Implementation of an adaptive position control system of a permanent-magnet synchronous motor and its application," IET Electr. Power Appl., vol. 4, no. 2, pp. 121–130, 2010.

[20] J. Jiang, X. Zhou, W. Zhao, and W. Li, "A model reference adaptive sliding mode control for the position control of permanent magnet synchronous motor," Proceedings of the Institution of Mechanical Engineers, Part I: Journal of Systems and Control Engineering, vol. 235, no. 3, pp. 389–399, 2021.

[21] Y. Guo and H. Long, "Self organizing fuzzy sliding mode controller for the position control of a permanent magnet synchronous motor drive," Ain Shams Engineering Journal, vol. 2, no. 2, pp. 109–118, 2011.

[22] W. Zhu, D. Chen, H. Du, and X. Wang, "Position control for permanent magnet synchronous motor based on neural network and terminal sliding mode control," Transactions of the Institute of Measurement and Control, vol. 42, no. 9, pp. 1632–1640, 2020.

[23] G.-Q. Ruan, Y.-Y. Su, J.-L. Cao, Y.-H. Su, Z.-D. Gong, and X. Hu, "Position tracking control of permanent magnet synchronous motor based on AHONFTSMC control," Journal of Electrical Engineering & Technology, vol. 20, no. 1, pp. 389–401, 2025.

[24] Z. Huang, S. Qiu, B. Wang, and Q. Liu, "High Precision and Fast Synchronization Fuzzy Position FPGA Based Controller for Smart-Multi-Motor System," IEEE Trans. Ind. Appl., 2025.

[25] J.-L. Shi, T.-H. Liu, and Y.-C. Chang, "Position control of an interior permanent-magnet synchronous motor without using a shaft position sensor," IEEE Transactions on Industrial Electronics, vol. 54, no. 4, pp. 1989–2000, 2007.

[26] Y. Yao, Y. Zhuang, Y. Xie, P. Xu, and C. Wu, "Prescribed performance global non-singular fast terminal sliding mode control of PMSM based on linear extended state observer," in Actuators, MDPI AG, 2025, p. 65.